



# Thermal conductivity of a-U with point defects

October 2021

*Changing the World's Energy Future*

Jie Peng, W.Ryan Deskins, Anter El Azab, Linu Malakkal



**DISCLAIMER**

This information was prepared as an account of work sponsored by an agency of the U.S. Government. Neither the U.S. Government nor any agency thereof, nor any of their employees, makes any warranty, expressed or implied, or assumes any legal liability or responsibility for the accuracy, completeness, or usefulness, of any information, apparatus, product, or process disclosed, or represents that its use would not infringe privately owned rights. References herein to any specific commercial product, process, or service by trade name, trade mark, manufacturer, or otherwise, does not necessarily constitute or imply its endorsement, recommendation, or favoring by the U.S. Government or any agency thereof. The views and opinions of authors expressed herein do not necessarily state or reflect those of the U.S. Government or any agency thereof.

# **Thermal conductivity of a-U with point defects**

**Jie Peng, W.Ryan Deskins, Anter El Azab, Linu Malakkal**

**October 2021**

**Idaho National Laboratory  
Idaho Falls, Idaho 83415**

**<http://www.inl.gov>**

**Prepared for the  
U.S. Department of Energy  
Under DOE Idaho Operations Office  
Contract DE-AC07-05ID14517**

# Thermal conductivity of $\alpha$ -U with point defects

Jie Peng <sup>1 a)</sup>, W. Ryan Deskins <sup>1</sup>, Linu Malakkal <sup>2</sup>, and Anter El-Azab <sup>1</sup>

<sup>1</sup> Materials Engineering, Purdue University, West Lafayette, Indiana 47907, USA

<sup>2</sup> Computational Mechanics and Materials Department, Idaho National Laboratory, Idaho Falls, Idaho 83415, USA

<sup>a)</sup> Author to whom correspondence should be addressed: [peng276@purdue.edu](mailto:peng276@purdue.edu)

## ABSTRACT

We develop a theoretical model for thermal conductivity of  $\alpha$ -U which combines density functional theory calculations and coupled electron-phonon Boltzmann transport equation. The model incorporates both electron and phonon contributions to thermal conductivity, achieves good agreement with experimental data over a wide temperature range. The dominant scattering mechanism governing thermal transport in  $\alpha$ -U at different temperatures is examined. By including phonon-defect and electron-defect scatterings in the model, we study the effect of point defects including U-vacancy, U-interstitial, and Zr-substitution on thermal conductivity of  $\alpha$ -U. The degradation of anisotropic thermal conductivity due to point defects as a function of defect concentration, defect type, and temperature is reported. This model provides insights into the impact of defects on both phonon and electronic thermal transport. It will promote the fundamental understanding of thermal transport in  $\alpha$ -U and provide a ground for investigation of coupled electron-phonon transport in metallic materials.

## 1. INTRODUCTION

Uranium is a crucial element in the actinide series that is widely used as a nuclear fuel in the fission reactor [1]. Uranium is not only one of the heaviest naturally occurring element on earth [2] but also an unique element where a charge density wave (CDW) state has been observed [1, 3,

4]. From 0 K to 43 K, it exhibits a series of low CDW transitions and stabilizes as the face-centered orthorhombic  $\alpha$  phase at 43 K and above. At higher temperature,  $\alpha$ -U transforms to  $\beta$  phase at around 933 K and then to the  $\gamma$  phase at around 1050 K [2]. Numerous studies have investigated the structural, electronic, optical properties, and phase stability of  $\alpha$ -U [1, 4, 5, 6, 7].

Determining the thermal properties of  $\alpha$ -U is crucial for its applications in nuclear reactors. However, compared to the large number of works studying the electronic and other ground-state properties of  $\alpha$ -U, relatively few studies focus on the thermal properties of  $\alpha$ -U. For the past few decades, the thermal conductivity data of  $\alpha$ -U was obtained primarily via experimental measurements [8, 9, 10, 11]. However, the high cost and limited accuracy of the experimental techniques make it difficult to obtain thermal conductivity data over a wide range of temperature and material conditions. Moreover, the thermal transport in  $\alpha$ -U depends on different scattering contributions: electron-electron scattering, phonon-phonon scattering, phonon-electron scattering, various defect scattering and so on. The available experimental techniques cannot distinguish the contributions of different scattering mechanisms towards the thermal conductivity. Therefore, it is essential to develop theoretical models not only to separate out phenomena but also to shed light into the fundamental physics of thermal transport in  $\alpha$ -U. To the best of our knowledge, the only thermal conductivity model of  $\alpha$ -U is found in a recent work by Shuxiang *et al.* [12]. However, Shuxiang's work evaluates electronic thermal conductivity using the Wiedemann-Franz law [13], known to break down for inelastic electron scattering processes [13, 14]. Moreover, this model includes parameters fitting of many experimental data, leading to uncertainty in the predicted thermal conductivity. The previous model's shortcoming warrants a more sophisticated theoretical model for the thermal conductivity of  $\alpha$ -U.

Point defects such as vacancies, interstitials, and substitutional atoms that alter the crystalline structures, have a detrimental effect on thermal conductivity of nuclear fuels. Several previous studies have reported the effect of point defects on thermal transport in Uranium compounds. For instance, a molecular dynamics (MD) simulations study reports the thermal conductivity degradation in uranium dioxide (UO<sub>2</sub>), as a function of defect concentration and temperature [15]. Another MD study [16] shows that a 0.1% U vacancy in UO<sub>2</sub> degrades the thermal conductivity by 24.6% [16]. The influence of carbon vacancies and oxygen substitutional impurities on thermal properties of uranium monocarbide (UC) was also studied within the density functional theory (DFT) [17]. Whereas, in the case of  $\alpha$ -U, the existing point defect studies on the defected crystals are limited to its structural, kinetics and the energetics properties [18, 19, 20]. A thorough investigation on the effect of point defects on thermal transport in  $\alpha$ -U seems to be still lacking. Thermal transport in  $\alpha$ -U is dominated by the electrons due to its metallic nature [12], therefore, it is critical to understand the electron-defect scatterings contributions in the thermal conductivity of defected  $\alpha$ -U. Nevertheless, in Shuxiang *et al.*'s thermal conductivity model of  $\alpha$ -U, the contribution from electron-defect scattering to thermal conductivity is represented by a constant value extracted from experimental data [12]. Thus, a more careful examination of the impact of point defects on electronic thermal transport in  $\alpha$ -U is necessary.

The present work develops a theoretical model of  $\alpha$ -U thermal conductivity that combines DFT calculations with Boltzmann transport equation (BTE) of coupled electron and phonon transport. The model developed here considers all electron- and phonon-scattering mechanisms governing thermal transport in  $\alpha$ -U, without including any fitting parameter from experimental data. We also go beyond the traditional Wiedemann-Franz law, which is commonly used in evaluating the electronic contribution to thermal conductivity in metals. The thermal conductivity

of pure  $\alpha$ -U crystal predicted by our model are in better agreement with the experimental data than the results obtained using the Wiedemann-Franz law. By including the phonon-defect and electron-defect relaxation times (RTs) into the thermal conductivity model of pure  $\alpha$ -U, the impact of different defects including U vacancy, U interstitial, and Zr substitution on the anisotropic thermal conductivity of  $\alpha$ -U as a function of defect type, defect concentration, and temperature is reported.

## 2. THERMAL CONDUCTIVITY MODEL

In metals, the primary heat carriers are electrons and phonons [13, 21]. Thus, the total thermal conductivity ( $\kappa$ ) can be expressed as

$$\kappa = \kappa_e + \kappa_{ph} \quad (1)$$

where the total thermal conductivity depends on various scattering processes involving electrons and phonons. In this work, phonon thermal conductivity  $\kappa_{ph}$  is affected by the phonon-phonon, phonon-electron, and phonon-defect scattering processes, while electronic thermal conductivity  $\kappa_e$  is influenced by the electron-phonon, electron-electron, and electron-defect scattering. Evaluation of  $\kappa_e$  and  $\kappa_{ph}$  requires harmonic properties of phonons, electronic band energy, and the RTs of the aforementioned scattering processes. In this section, a detailed description of the model used for calculating the thermal conductivity of  $\alpha$ -U is presented.

### 2.1 Phonon thermal conductivity

The phonon thermal conductivity  $\kappa_{ph}$  is formulated within the phonon BTE framework as [13, 22]

$$\vec{\kappa}_{ph} = \sum_{vq} C_{vq} \vec{v}_{vq} \otimes \vec{v}_{vq} \tau_{vq}^{ph} \quad (2)$$

where the index  $\nu q$  refers to the phonon mode with branch index  $\nu$  at wavevector  $q$ ,  $C_{\nu q}$  is the phonon volumetric specific heat capacity,  $\vec{v}_{\nu q}$  is the phonon group velocity, and  $\tau_{\nu q}^{ph}$  is the phonon RT. By discretizing the Brillouin zone (BZ) into a grid that contains  $N_q$  number of  $q$  points, the mode-dependent phonon specific heat  $C_{\nu q}$  can be calculated using the phonon dispersion [23]

$$C_{\nu q}(\omega_{\nu q}, T) = \frac{k_B}{N_q V} \left( \frac{\hbar \omega_{\nu q}}{k_B T} \right)^2 \frac{e^{-\frac{\hbar \omega_{\nu q}}{k_B T}}}{\left( e^{-\frac{\hbar \omega_{\nu q}}{k_B T}} - 1 \right)^2} \quad (3)$$

where  $k_B$  is the Boltzmann constant,  $V$  is the volume of the unit cell,  $\hbar$  is the Planck constant, and  $\omega_{\nu q}$  is the phonon frequency. The group velocity is also calculated using the phonon dispersion as

$$\vec{v}_{\nu q} = \frac{\partial \omega_{\nu q}}{\partial \vec{q}}.$$

The phonon RT combining all scattering processes can be calculated using the Matthiessen's rule [21, 24]

$$\frac{1}{\tau_{\nu q}^{ph}} = \frac{1}{\tau_{\nu q}^{ph-ph}} + \frac{1}{\tau_{\nu q}^{ph-e}} + \frac{1}{\tau_{\nu q}^{ph-d}} \quad (4)$$

where  $\tau_{\nu q}^{ph-ph}$ ,  $\tau_{\nu q}^{ph-e}$ , and  $\tau_{\nu q}^{ph-d}$  are the RTs of phonon-phonon, phonon-electron, and phonon-defect scattering processes, respectively. The relatively rare cases when the Matthiessen's rule fail are beyond the interests of this work.

For the phonon-phonon scattering, we limit our discussion to three-phonon processes. The higher order scattering processes are important when the higher order scattering potential or phase space becomes relatively large [25], usually for strongly anharmonic materials or at very high temperature. In this work, we deem that the contributions from these higher order scattering processes to thermal transport in  $\alpha$ -U at the temperature range of interests would be small. The

ShengBTE code was used [22] to calculate the three-phonon scattering RTs. For simplicity, let  $g = \nu q$  represents a phonon mode. The RT  $\tau_{\nu q}^{ph-ph}$  includes contributions from the phonon absorption and emission processes [22],

$$\frac{1}{\tau_g^{ph-ph}} = \frac{1}{N_q} \left( \sum_{g'g''}^+ \Gamma_{gg'g''}^+ + \frac{1}{2} \sum_{g'g''}^- \Gamma_{gg'g''}^- \right) \quad (5)$$

where  $\Gamma_{gg'g''}^+$  and  $\Gamma_{gg'g''}^-$  represents the scattering rates of the fusion and fission processes, respectively. The scattering rates can be calculated using the scattering matrix  $\Psi_{gg'g''}^\pm$  as

$$\Gamma_{gg'g''}^+ = \frac{\hbar\pi}{4} \cdot \frac{n'_0 - n''_0}{\omega_g \omega_{g'} \omega_{g''}} \left| \Psi_{gg'g''}^+ \right|^2 \delta(\omega_g + \omega_{g'} - \omega_{g''}) \quad (6)$$

$$\Gamma_{gg'g''}^- = \frac{\hbar\pi}{4} \cdot \frac{n'_0 + n''_0 + 1}{\omega_g \omega_{g'} \omega_{g''}} \left| \Psi_{gg'g''}^- \right|^2 \delta(\omega_g - \omega_{g'} - \omega_{g''})$$

where  $n'_0 = n_0(\omega_{g'}) = 1/(e^{\hbar\omega_{g'}/k_B T} - 1)$  represents phonon distribution at equilibrium which obeys the Bose-Einstein statistics. The conservation of energy in the absorption and emission processes is enforced by the Dirac delta function in Eq. (6). Finally, the scattering matrix can be calculated from the third-order force constants and phonon eigenvectors [22, 26]

$$\Psi_{gg'g''}^\pm = \sum_i \sum_{jk} \sum_{\alpha\beta\gamma} \Phi_{ijk}^{\alpha\beta\gamma} \frac{e_g^\alpha(i) e_{g'}^\beta(j) e_{g''}^\gamma(k)}{\sqrt{M_i M_j M_k}} \quad (7)$$

where  $ijk$  are the atomic indices,  $\alpha\beta\gamma$  denote Cartesian coordinates,  $e_g^\alpha(i)$  represents the  $\alpha$  component of the eigenvector of phonon mode  $g$  at the  $i^{th}$  atom,  $M_i$  is the mass of the  $i^{th}$  atom, and  $\Phi_{ijk}^{\alpha\beta\gamma}$  is the third-order force constant matrix.

The phonon-electron RT is estimated by Pippard's theory [21, 27]

$$\frac{1}{\tau_{\nu q}^{ph-e}} = \frac{\pi n_e m v_F}{6d v_{\nu q}} \omega_{\nu q} \quad (8)$$

where  $n_e$  is the electron density,  $m$  is the electron mass,  $v_F$  is electron Fermi velocity, and  $d$  is the ionic mass density. The Pippard's formula has been used to predict phonon thermal conductivity of Cu alloy [28], Ni-doped CoSb<sub>3</sub> [29], and transition metal carbides [30] where phonon-electron scatterings play an important role in determining the thermal conductivity.

For phonon-defect scatterings, the RT is given by Klemens [31]

$$\frac{1}{\tau_{\nu q}^{ph-d}} = \frac{G V_a}{4\pi v_{\nu q}^3} \omega_{\nu q}^4 \quad (9)$$

where  $V_a$  is the average atomic volume at the defect site and  $G$  is the phonon-defect scattering parameter. In the case of a single element material like  $\alpha$ -U, the scattering parameter can be calculated by [32]

$$G = \sum_i n_d^i \left[ \frac{\langle \overline{\Delta M^2} \rangle}{\langle \overline{M^2} \rangle} + 2 \left( \frac{\langle \overline{\Delta K} \rangle}{\langle \overline{K} \rangle} - 2Q\gamma \frac{\langle \overline{\Delta R} \rangle}{\langle \overline{R} \rangle} \right)^2 \right] \quad (10)$$

where  $n_d^i$  is the fractional defect concentration at the  $i$ th atomic site,  $Q$  is the number of distorted nearest-neighbor bonds around the defect (3.2 for substitutional defect and 4.2 for vacancies),  $\Delta M$ ,  $\Delta K$ , and  $\Delta R$  are the mass difference, harmonic force constant difference, and atomic radius difference of the defected site. In Eq. (10), the atomic site averages are denoted with a bar, while the stoichiometric averages are denoted with angled brackets. The average mass variance and average mass are given by

$$\overline{\Delta M^2} = \sum_i n_d^i (M_i - \bar{M})^2, \bar{M} = \sum_i n_d^i M_i \quad (11)$$

For vacancy and interstitial defects of which the perturbation is due to both mass difference and removal/creation of nearest neighbor bonds, the virial theorem drops the potential terms and modifies the change in mass at a vacancy site as  $M_i - \bar{M} = -M_{vac} - 2\bar{M}$  and at an interstitial site as  $M_i - \bar{M} = M_{int} + 2\bar{M}$  [33].

## 2.2 Electronic thermal conductivity

The expression for calculating the electronic thermal conductivity in metals can be derived from the linearized BTE of electrons [13, 34]. Under the RT approximation, the transport distribution function is given by

$$\Xi(\epsilon, T) = \int \sum_{bk} v_{bk} \otimes v_{bk} \tau_{bk}^e \delta(\epsilon - \epsilon_{bk}) \frac{dk}{(2\pi)^3} \quad (12)$$

where  $\epsilon_{bk}$  is the electronic band energy,  $v_{bk}$  is the electronic group velocity, and  $\tau_{bk}^e$  is the RT for electron scattering processes. Using the transport distribution function, the generalized transport coefficients  $\mathcal{L}_0$ ,  $\mathcal{L}_1$ , and  $\mathcal{L}_2$  can be calculated as

$$\begin{aligned} \mathcal{L}_p(\mu, T) &= e^2 \int \Xi(\epsilon, T) (\epsilon - \mu)^p \left( -\frac{\partial f^0(\epsilon; \mu, T)}{\partial \epsilon} \right) d\epsilon \\ &= \frac{e^2 n_k}{V} \sum_{bk} (\epsilon_{bk} - \mu)^p \left( -\frac{\partial f_{bk}^0}{\partial \epsilon} \right) v_{bk} \otimes v_{bk} \tau_{bk}^e, \text{ for } p = 0, 1, 2 \end{aligned} \quad (13)$$

with  $f^0(\epsilon; \mu, T)$  being the Fermi-Dirac distribution function,  $\mu$  being the chemical potential which in metals is usually taken as the Fermi energy  $\mu = E_F$  [21],  $e$  is the elementary charge, and  $n_k$  is the number of  $k$  points in the BZ. The electrical and heat current is then given by the transport coefficients as

$$\vec{J}_e = \mathcal{L}_0 \vec{E} + \frac{\mathcal{L}_1}{eT} (-\vec{\nabla}T) \quad (14)$$

$$\vec{j}_Q = \frac{\mathcal{L}_1}{e} \vec{E} + \frac{\mathcal{L}_2}{e^2 T} (-\vec{\nabla} T)$$

with  $\vec{E}$  the external electrical field and  $\vec{\nabla} T$  the temperature gradient. By setting the electrical current and thermal gradient to zero in Eq. (14) respectively, the electronic thermal conductivity and electrical conductivity is finally obtained as

$$\sigma = \mathcal{L}_0 \quad (15)$$

$$\kappa_e = \frac{1}{e^2 T} \left[ \frac{\mathcal{L}_1^2}{\mathcal{L}_0} - \mathcal{L}_2 \right] \quad (16)$$

The  $\kappa_e$  can be calculated using Eq. (13) and (16) where the electronic band structure and RT corresponding to various electron scatterings are used as inputs. There are two RTs for electrons –  $\tau_{bk,\kappa}^e$  responsible for thermal relaxation of electrons which is used in Eq. (16) and  $\tau_{bk,\sigma}^e$  responsible for electronic relaxation of electrons which is used in Eq. (15). Two approaches can be adopted to calculate  $\kappa_e$ .

In the first approach, one considers  $\tau_{bk,\kappa}^e = \tau_{bk,\sigma}^e$  when the scattering mechanisms involving electrons are elastic. By dividing Eq. (16) by Eq. (15), the Lorenz number is defined as

$$L = \frac{\kappa_e}{\sigma T} = \frac{1}{e^2 T^2} \left[ \left( \frac{\mathcal{L}_1}{\mathcal{L}_0} \right)^2 - \frac{\mathcal{L}_2}{\mathcal{L}_0} \right] \quad (17)$$

Letting  $\tau_{bk,\kappa}^e = \tau_{bk,\sigma}^e$ , adopting free electron gas assumption, and neglecting the higher order term in Eq. (17), the famous Wiedemann-Franz law is obtained [13]

$$\frac{\kappa_e}{\sigma T} = L_0 = \frac{\pi^2}{3} \left( \frac{k_B}{e} \right)^2 = 2.4453 \times 10^{-8} W\Omega/K^2 \quad (18)$$

where the ratio of the electronic thermal conductivity to electrical conductivity is proportional to the absolute temperature, and the proportionality constant is the Sommerfeld value  $L_0$  [35] for the

Lorenz number. In this work, we refer to this approach as the WF approach, signifying the use of the Wiedemann-Franz law. To calculate  $\kappa_e$ , the electrical conductivity ( $\sigma$ ) is calculated using the Drude theory,

$$\sigma = \frac{n_e e^2}{m} \tau_\sigma^e \quad (19)$$

Here,  $\tau_{bk,\sigma}^e$  is written as  $\tau_\sigma^e$ , since in this work, isotropic RTs for all the electron scattering processes are considered. The obtained electrical conductivity  $\sigma$  is then used to calculate  $\kappa_e$  using Eq. (18).

The Wiedemann-Franz law is usually well obeyed at high temperatures. However, it has been shown to fail at low- and intermediate-temperatures when electrons participate in inelastic scattering events [13, 14]. In these situations, it is essential to distinguish between the electronic and thermal RTs of electron scatterings.

In the second approach, one considers  $\tau_{bk,\kappa}^e \neq \tau_{bk,\sigma}^e$  for electron scattering processes. The transport coefficients are evaluated first using Eq. (13). In determining the electrical conductivity  $\sigma$ , the transport coefficient  $\mathcal{L}^0$  is calculated using the electronic RT,  $\tau_\sigma^e$ . On the other hand, in determining the electronic thermal conductivity  $\kappa_e$ , the transport coefficients  $\mathcal{L}^p$  ( $p = 0,1,2$ ) are calculated using the thermal RT,  $\tau_\kappa^e$ . We refer to this approach as the TC approach to indicate the use of the transport coefficients.

For both WF and TC approach, the electron RTs - both  $\tau_\kappa^e$  and  $\tau_\sigma^e$  - can be calculated using Matthiessen's rule [21, 24]

$$\frac{1}{\tau_{\kappa(\sigma)}^e} = \frac{1}{\tau_{\kappa(\sigma)}^{e-ph}} + \frac{1}{\tau_{\kappa(\sigma)}^{e-e}} + \frac{1}{\tau_{\kappa(\sigma)}^{e-d}} \quad (20)$$

where  $\tau_{\kappa(\sigma)}^{e-ph}$ ,  $\tau_{\kappa(\sigma)}^{e-e}$ , and  $\tau_{\kappa(\sigma)}^{e-d}$  are the thermal (electronic) RTs of electron-phonon, electron-electron, and electron-defect scattering processes, respectively.

Considering the electron-phonon scattering, the RT is determined by the coupling function for the electron-phonon interaction. By treating electrons as free electrons and limiting the available phonons for electron-phonon scattering in the long-wavelength limits, the coupling function  $C_{e-ph}$  is given by [36]

$$C_{e-ph} = \sqrt{\lambda \frac{\pi^2 \hbar^3 \omega_{\nu q}}{m k_F}} \quad (21)$$

where  $k_F$  is the Fermi wavevector. The dimensionless parameter  $\lambda$  is calculated as

$$\lambda = \frac{2Zm}{3M} \left( \frac{E_F}{k_B \Theta_s} \right)^2 \quad (22)$$

where  $Z$  is the ionic charge and  $E_F$  is the Fermi energy. The temperature  $\Theta_s = \frac{v_s \hbar k_F}{k_B}$  represents the Bloch-Grüneisen temperature [37, 38] where  $v_s$  is the group velocity of longitudinal acoustic phonons in the long-wavelength limit. Using the coupling function obtained from Eq. (21), the RT can be calculated from the collision integral of the electron BTE. The detailed derivation is found in [21, 36], from which the electronic and thermal RTs are given as [36]

$$\frac{1}{\tau_{\sigma}^{e-ph}} = \frac{\pi}{2} \lambda \frac{k_B T^5}{\hbar \Theta_s^4} J_5 \quad (23)$$

$$\frac{1}{\tau_{\kappa}^{e-ph}} = \frac{\pi}{2} \lambda \frac{k_B T^5}{\hbar \Theta_s^4} J_5 \left( 1 + \frac{3\Theta_s^2}{\pi^2 T^2} - \frac{J_7}{2\pi^2 T^2} \right) \quad (24)$$

where  $J_n = \int_0^{\frac{2\Theta_s}{T}} \frac{x^n}{4 \sinh^2(\frac{x}{2})} dx$ .

The electronic and thermal RT for electron-electron scattering is [21, 39, 40]

$$\frac{1}{\tau_{\kappa}^{e-e}} = \frac{1}{\tau_{\sigma}^{e-e}} = \frac{e^4 (k_B T)^2}{16\pi\hbar^4 \epsilon_0^2 k_F v_F^3} \left[ 1 + \left( \frac{E_F}{\pi k_B T} \right)^2 \right] Y \left( \frac{2k_F}{k_{TF}} \right) \quad (25)$$

where  $\epsilon_0$  is vacuum permittivity,  $v_F$  is electron Fermi velocity,  $k_{TF} = \sqrt{\frac{4k_F m \epsilon^2}{\pi\hbar^2}}$  is the Thomas-Fermi screening parameter and the analytical function  $Y(x) = \frac{x^3}{4} [\tan^{-1} x + \frac{x^2}{1+x^2} - \frac{1}{\sqrt{2+x^2}} \tan^{-1} x \sqrt{2+x^2}]$ . Eq. (25) has been applied to estimate electrical resistivity of a number of metals including Al, Mg, In, and so on [40].

Finally, the electronic and thermal electron-defect RT due to a static charged defect of valance  $Z$  that occupies a lattice site is given by [21]

$$\frac{1}{\tau_{\kappa}^{e-d}} = \frac{1}{\tau_{\sigma}^{e-d}} = \frac{2\pi n_d E_F Z^2}{3\hbar n_e} F \left( \frac{2k_F}{k_{TF}} \right) \quad (26)$$

where the function  $F(x) = \frac{2[\ln(1+x) - x/(1+x)]}{x^2}$ . Through a screened Coulomb interaction, the electric field generated by the charged defect drives the electrons to redistribute around the defect site and perturbs the ion-electron potential energy. The expression of  $\tau_{\kappa}^{e-d}$  is derived using the perturbation potential energy. Eq. (26) was used to calculate the change in electrical resistivity of Cu due to Ag and Au defects and compares well with experimental data [21]. In this work, all defects are considered as charged defects.

### 3 COMPUTATIONAL DETAILS

In this section, we present the details of the computational procedure. DFF was used to compute the phonon and electronic band structure required for the thermal conductivity calculations, as well as the anharmonic force constants required as input in phonon-phonon scattering rates. All the DFT calculations were performed using VASP [41]. Initial lattice constants and atomic coordinates for the  $\alpha$ -U unit cell was taken from X-ray diffraction experiments

conducted at 298K [5]. The exchange-correlation functional with the Perdew, Burke, and Ernzerhof (PBE) [42] form under the Generalized Gradient Approximation (GGA) [43] was chosen. The cutoff energy for the plane-wave basis set was set to 450 eV and the first Brillouin zone (BZ) was sampled with a  $8 \times 8 \times 8$  Monkhorst-Pack k-point mesh grid. For lattice structural relaxation, the conjugate-gradient algorithm was used where the stopping criteria for self-consistent electronic loop and ionic relaxation were set to 0.1 and 1 meV, respectively. Density functional perturbation theory (DFPT) [44] as implemented in the VASP code was used for the calculation of phonon properties. The phonon dispersion spectra were obtained using the Phonopy code [45], considering a  $4 \times 4 \times 4$  supercell and a  $4 \times 4 \times 4$  Monkhorst-Pack q-point mesh grid. For electronic band structure calculations, a  $10 \times 10 \times 10$  Monkhorst-Pack k-point mesh grid was used. For the phonon-phonon RT calculations where third-order force constant matrix is needed, an auxiliary python module *thirdorder.py* in the ShengBTE code [22] was used. The anharmonic force constants were calculated using a  $4 \times 4 \times 4$  supercell. For all the other RTs, the required parameters were extracted from the already obtained phonon dispersion, electronic band structure, and ground-state data such as Fermi energy, Fermi velocity, and so on.

To study the impact of defects on thermal transport in  $\alpha$ -U, three different defects are considered: U-vacancy, U-interstitial, and Zr-substitution. A defected lattice site is created in  $3 \times 3 \times 3$ ,  $4 \times 4 \times 4$ , and  $5 \times 5 \times 5$  U supercells for each defect, resulting in defect concentration of  $n_d = 0.4\%$ ,  $0.78\%$ , and  $1.85\%$ , respectively. The supercell shape and internal atomic coordinates of all the defected supercells were relaxed to obtain equilibrium configuration. The Monkhorst-Pack k-point mesh used in the relaxation were  $4 \times 4 \times 4$ ,  $4 \times 4 \times 4$ , and  $2 \times 2 \times 2$  for the  $3 \times 3 \times 3$ ,  $4 \times 4 \times 4$ , and  $5 \times 5 \times 5$  supercells, respectively. For Zr-substitution in  $\alpha$ -U, we adopted DFT+U functional [46], which has been shown to produce more accurate total energy

and lattice structure for U-Zr systems than the standard DFT [47]. The VASP inputs for DFT+U functional were set as  $U = 1.75$  and  $J = 0.51$ , which are the same setting as a previous study on electronic and structural properties of U-Zr system [47]. The force constants at the defected lattice site were calculated by moving the target atom from its equilibrium position from  $-0.05 \text{ \AA}$  to  $0.05 \text{ \AA}$  in increment of  $0.01 \text{ \AA}$ , along three cartesian directions. The resultant energy-displacement curves were fit to second-order polynomials where the coefficients were taken as half of the force constants.

## 4 RESULTS AND DISCUSSION

### 4.1 Lattice structure

The  $\alpha$ -U crystal has a face-centered orthorhombic structure with two atoms per primitive unit cell (space group:  $Cmcm$ , No. 63), as shown in Figure 1. The conventional unit cell contains four atoms at  $4c$ ,  $(0, y, 0.25)$  Wyckoff positions. In Table 1, we list the lattice parameters and fractional coordinates of the atoms from our DFT calculations compared to other published results. Our calculated lattice parameters are well within the range of other theoretical calculations. The lattice parameters  $a$ ,  $b$ ,  $c$ , and volume per atom is only slightly smaller compared to the experimental data. We conclude that the crystal structure of  $\alpha$ -U is well reproduced by our DFT calculation.

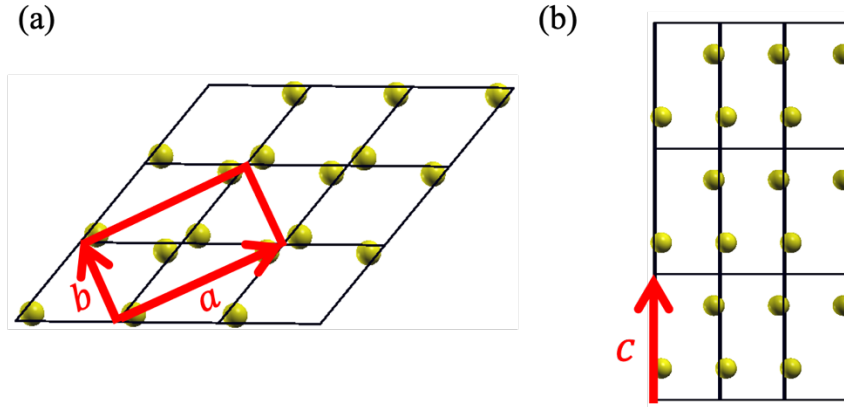


Figure 1. (a) Top view and (b) side view of the lattice configuration of a  $3 \times 3 \times 3$   $\alpha$ -U supercell. The primitive unit cell is represented by the black boxes, each consisting of two U atoms. The red lines outline the orthorhombic unit cell, with the lattice parameters  $a$ ,  $b$ , and  $c$  represented by the red arrows.

**Table 1.** Lattice parameters ( $a$ ,  $b$ , and  $c$ ), the fractional coordinate of the atoms ( $y$ ), and atomic volume of  $\alpha$ -U from simulations (Sim), experiments (Exp), and this work.

	Reference	$a$ (Å)	$b$ (Å)	$c$ (Å)	$y$	Volume/atom (Å <sup>3</sup> )
Sim	PBE-DFT [48]	2.793	5.849	4.894	0.098	19.987
	PW91-DFT [49]	2.8	5.896	4.893	0.097	20.194
	Full-potential [6]	2.845	5.818	4.996	0.103	20.674
	LDA-DFT [50]	2.809	5.447	4.964		19.026
	PBE-DFT [12]	2.794	5.844	4.913	0.098	20.057
Exp	T=4.2 K [5]	2.844	5.869	4.932	0.102	20.535
	T=298 K [51]	2.854	5.87	4.956		20.751
	T=298 K [52]	2.8553	5.8701	4.9568		20.77
Present work	PBE-GGA DFT	2.817	5.867	4.875	0.098	19.99

## 4.2 Phonon dispersion and electronic band structure

In our thermal conductivity model, the accuracy of the phonon dispersion and electronic band structure data is important. In Figure 2, the calculated phonon dispersion and density of states (DOS) are compared with other published results. Our results agree well with experimental data along the [100] direction [53, 54, 55, 56]. Specifically, the phonon frequencies and the slope of the dispersion of the acoustic branches near the  $\Gamma$  point show excellent agreement with the experimental data. Large discrepancies between theory and experimental dispersion data of the

optical branches along the [010] and [001] are observed. These optical branches obtained from other DFT calculations [56, 57] also show similar discrepancies in comparison to the experimental data. The possible explanations include large uncertainty in the measurements for these modes [53, 56], the temperature difference between our DFT calculations (0K) and experiments (300K), and the charge-density-wave transition which could potentially affect the optical phonons [1]. Figure 3 shows our calculated electronic band structure and DOS, which agrees well with other DFT calculations [47] and experimental measurements [58].

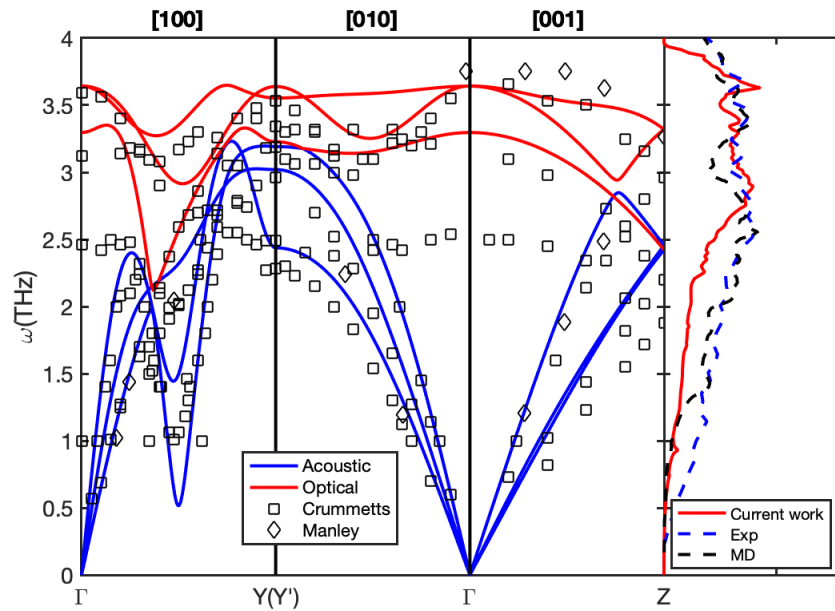


Figure 2. Phonon dispersion curves and DOS calculated using Phonopy and VASP. The dispersion is compared with Crummette’s inelastic neutron scattering measurements data [53] and Manley’s X-ray scattering measurements data [54]. The DOS data is compared with data obtained from neutron scattering experiments (Exp) at 50K [55] and MD simulation [59].

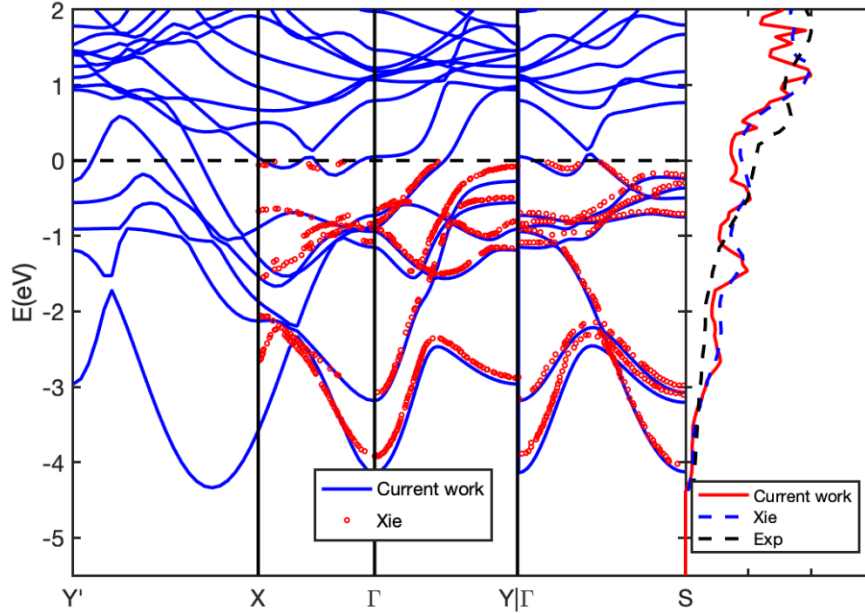


Figure 3. Electronic band structure and DOS of  $\alpha$ -U. The electronic bands are compared with results obtained from other DFT calculations [47]. The DOS data is compared with DFT calculations [47] and X-ray photoemission spectroscopy measurements [58].

### 4.3 Thermal properties of defect-free $\alpha$ -U

The thermal conductivity of defect-free  $\alpha$ -U serves as a reference point to investigate the effect of defects on thermal transport. We calculate the thermal conductivity of  $\alpha$ -U from 43K to 933K and show the results in Figure 4(a, b). Overall, the thermal conductivity calculated using the TC approach agrees better with experimental data than the WF approach. The two main reasons for the difference between  $\kappa_e$  obtained from the TC and WF approaches are: firstly, complete information of the electronic band structure is incorporated into the calculation of  $\kappa_e$  in the TC approach by Eq. (13) and (16), while the complex electronic band structure is overly simplified as the classical free electron gas model in the WF approach, leading to inaccurate value of  $\kappa_e$ . Secondly, in the WF approach, the Sommerfeld value of the Lorenz number is used, whereas, in the TC approach, the Lorenz number is temperature dependent. We plot the Lorenz number in the

WF and TC approach in Figure 4(c). It is seen that the Lorenz numbers along three directions are all temperature dependent, and rarely equals the classical Sommerfeld value. It has already been shown that the Lorenz number is temperature-dependent and varies with different materials [60, 61]. As pointed out by Ziman and Kittel, the Lorenz number for metals can deviate from the Sommerfeld value due to different RTs of electron scattering processes in electrical and thermal transport [62, 13]. Hence, we conclude that for evaluating electronic thermal conductivity of  $\alpha$ -U, one should adopt the TC method instead of the WF approach. For the rest of this paper, the results presented are all obtained using the TC approach. In Figure 4(d), specific heat from phonon and electronic contributions are shown. The phonon-specific heat shows a  $T^{-3}$  dependence at low temperatures and approaches the Dulong-petit limit (around 25 J/mol/K) at high temperatures. The electronic specific heat depends linearly on temperature, with the linear coefficient  $\gamma = 5.3 \times 10^{-3}$  J/mol/K comparable to other metals such as Fe and Co [14]. The total specific heat from our DFT calculation agrees well with the experimental data from 43 K to 350 K. Our calculated specific heat values from 350 K to 933 K could aid the future experimental measurements on the  $\alpha$ -U specific heat.

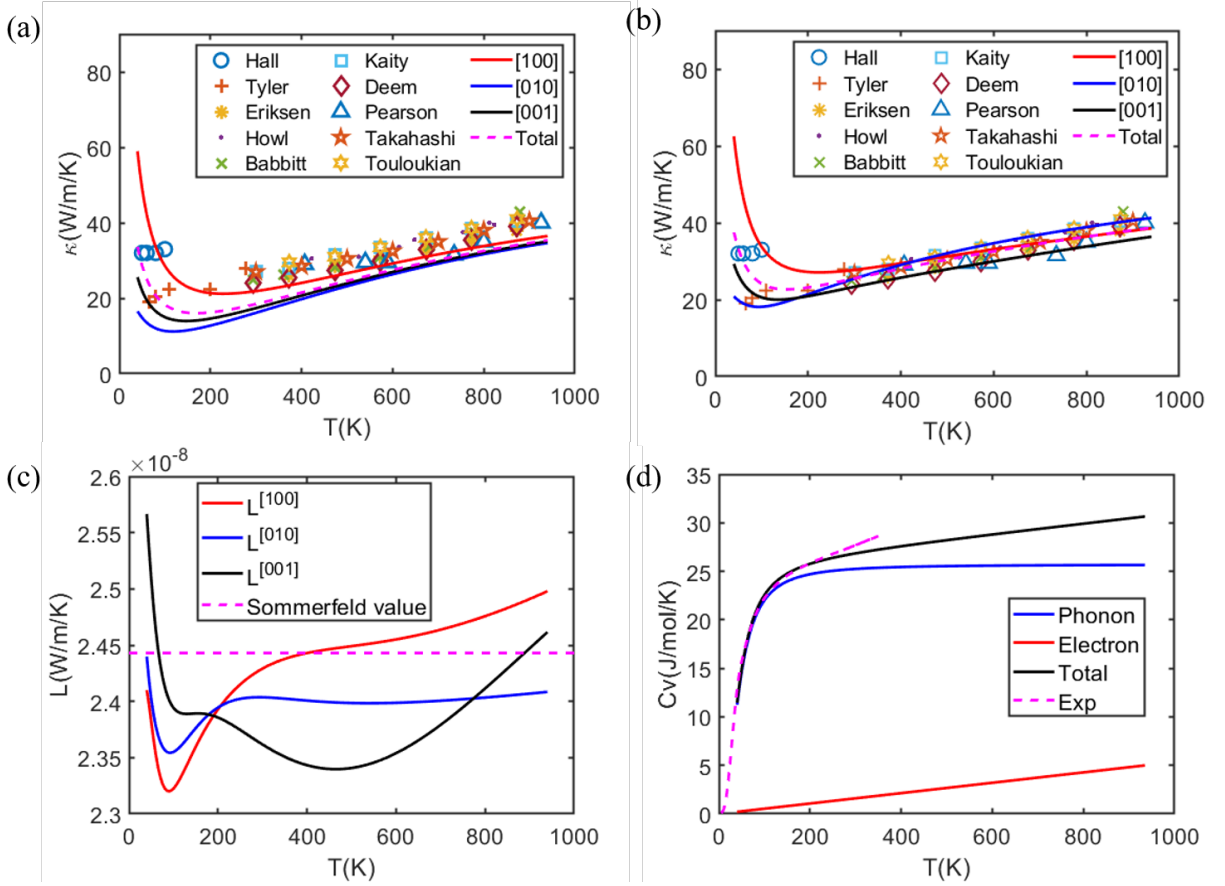


Figure 4. Thermal conductivity of defect-free  $\alpha$ -U using the (a) WF and (b) TC approach from 43K to 933K. The solid lines represent thermal conductivity along [100], [010], and [001] directions, while the dashed line represents total thermal conductivity  $\kappa_{\text{tot}} = \frac{1}{3}(\kappa_{[100]} + \kappa_{[010]} + \kappa_{[001]})$ . The scatter points represent experimentally measured thermal conductivity values [9, 8, 63, 64, 11, 65, 10]. (c) Lorenz number obtained from TC approach along three directions. The dashed line represents the Sommerfeld value used to determine  $\kappa_e$  from  $\sigma$  in the WF approach. (d) The total, phonon, and electronic volumetric specific heat from our DFT calculations compared to experimental measurements data [66].

To distinguish between the electron and phonon contributions towards the total thermal conductivity, we plot  $\kappa_e$  and  $\kappa_{ph}$  as a function of temperature in Figure 5(a). At low temperatures, phonon transport dominates the thermal transport in  $\alpha$ -U along all three directions. As temperature increases, phonons are scattered more frequently by phonons and electrons, resulting in a continuous decrease in phonon thermal conductivity. On the other hand, as temperature rises, the population of excited electrons increases, resulting in increasing  $\kappa_e$ . Phonons and electrons make

almost equal contributions to thermal conductivity along [100], [010], and [001] directions at 175 K, 60 K, and 100 K, respectively. Therefore, electrons are major heat carriers at room temperature and above and dominate the thermal transport in  $\alpha$ -U, which agrees with the other DFT model of  $\alpha$ -U thermal conductivity [12]. The thermal conductivity of  $\alpha$ -U exhibits temperature-dependent anisotropy, as is shown in Figure 5(b). Both our and Shuxiang *et al.*'s [12] results show that the anisotropy of thermal conductivity decreases with increasing temperature. Thermal conductivity tends to be more isotropic at high temperatures. For phonon thermal conductivity  $\vec{\kappa}_{ph}$ , at low temperatures, most of the excited phonons are low energy, acoustic phonons with different magnitude of group velocities along different directions, as is shown in Figure 2. Thus, the calculated  $\vec{\kappa}_{ph}$  according to Eq. (2) shows strong anisotropy. As temperature increases, more higher energy phonons are excited, of which the group velocity magnitude becomes less directional dependent. As a result, the anisotropy decreases. For the electronic thermal conductivity  $\vec{\kappa}_e$ , as temperature rises, the difference among the electron velocities along three directions is amplified in calculating the generalized transport coefficients  $\mathcal{L}_0$ ,  $\mathcal{L}_1$ , and  $\mathcal{L}_2$  according to Eq. (13). As a result, the electronic thermal conductivity becomes more directional-dependent.

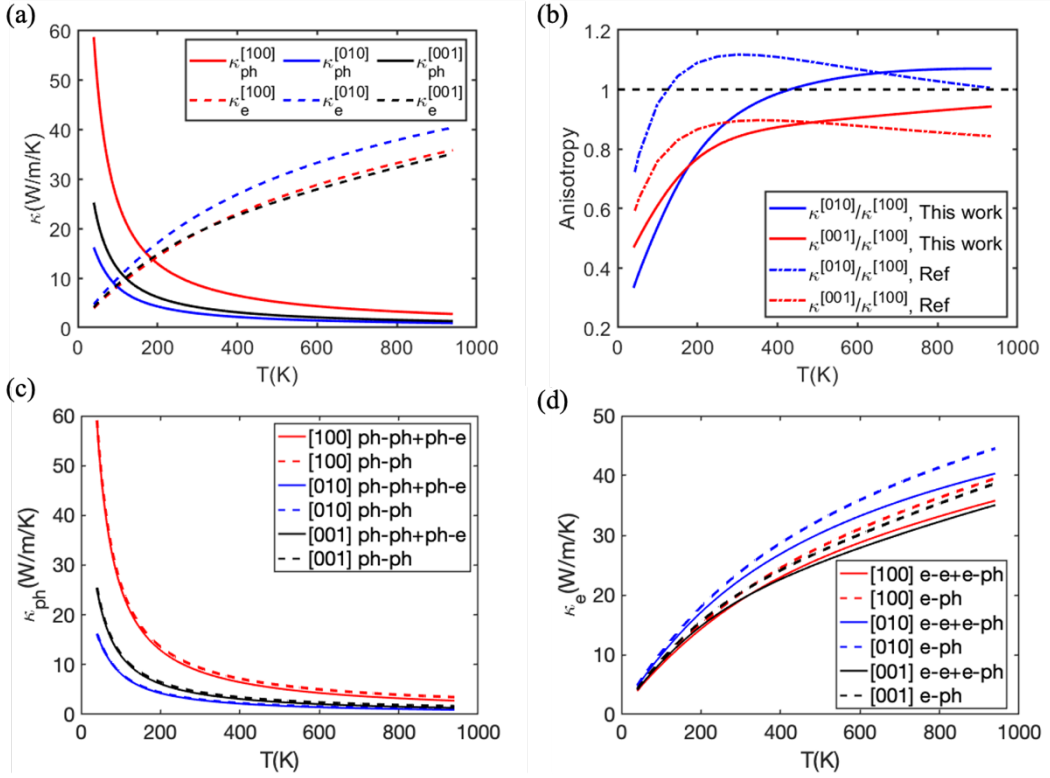


Figure 5. (a) Phonon and electronic thermal conductivity along three directions. (b) Thermal conductivity anisotropy of  $\alpha$ -U from our and Shuxiang *et al.*'s DFT [12] calculations. (c) Phonon thermal conductivity calculated using only  $1/\tau_{vq}^{ph-ph}$  (dashed lines) and using both  $1/\tau_{vq}^{ph-ph}$  and  $1/\tau_{vq}^{ph-e}$  (solid lines) in Eq. (4). (d) Electronic thermal conductivity calculated using  $1/\tau_{\kappa}^{e-ph}$  only (dashed lines) and using both  $1/\tau_{\kappa}^{e-ph}$  and  $1/\tau_{\kappa}^{e-e}$  (solid lines) in Eq. (20).

Figure 5(c) shows the impact of phonon-electron scatterings on the phonon thermal conductivity, by displaying the impact of the phonon-phonon process (dashed lines) versus the phonon-phonon plus the phonon-electron process (solid lines). The figure shows that adding the phonon-electron scattering degrades the thermal conductivity by only a small amount at all temperatures. At room temperature, the phonon-electron scatterings only reduce the conductivity by about 7.6%, 3%, and 7.3% relative to the phonon thermal conductivity along [100], [010], and [001] directions, respectively, when considered in addition to the phonon-phonon process. A similar conclusion has been drawn in other metals such as Al and Ag, where the effect of phonon-

electron scatterings on phonon thermal conductivity is negligible above room temperature [67]. Therefore, we conclude that the phonon-phonon scatterings dominate the phonon thermal conductivity of  $\alpha$ -U at all temperatures. Figure 5(d) shows the impact of electron-electron and electron-phonon scattering on the electronic thermal conductivity, by displaying the impact of the electron-electron plus the electron-phonon processes (solid lines) versus the electron-phonon process alone (dashed lines). With the electron-electron scattering added to the electron-phonon scattering, the electronic thermal conductivity is only reduced slightly at all temperatures. Therefore, the electronic thermal transport in  $\alpha$ -U is dominated by the electron-phonon scatterings. The electrons scattering by phonons thus plays a decisive role in determining the electronic thermal conductivity whereas the phonons scattering by electrons has negligible influence on the phonon thermal conductivity.

#### 4.4 Effect of point defects on thermal conductivity

The lattice configurations of U-vacancy, U-interstitial, and Zr-substitution defected  $\alpha$ -U supercells obtained from DFT calculations are shown in Figure 6. The vacancy and substitution defects are created on the U atomic sites. For the U-interstitial, the U interstice is placed at the so-called free space site, as is shown in Figure 6(b) [68]. Among the four possible interstitial sites around a lattice site in  $\alpha$ -U unit cell: free space, the [100], [010], and [001] split dumbbell interstitials, the free space interstitial defected lattice configuration has the lowest formation energy and thus more energetically favorable when an interstitial defect is created [68, 69]. The structural properties of the defected supercell and the formation energy of defects are listed in Table 2. Our calculated defect formation energies agree well with other published results. The formation energy of the U-interstitial (4.9 eV) is much larger than the value of vacancy (1.9 eV) due to the large atomic radius of U and the close-packed nature of the lattice structure [69].

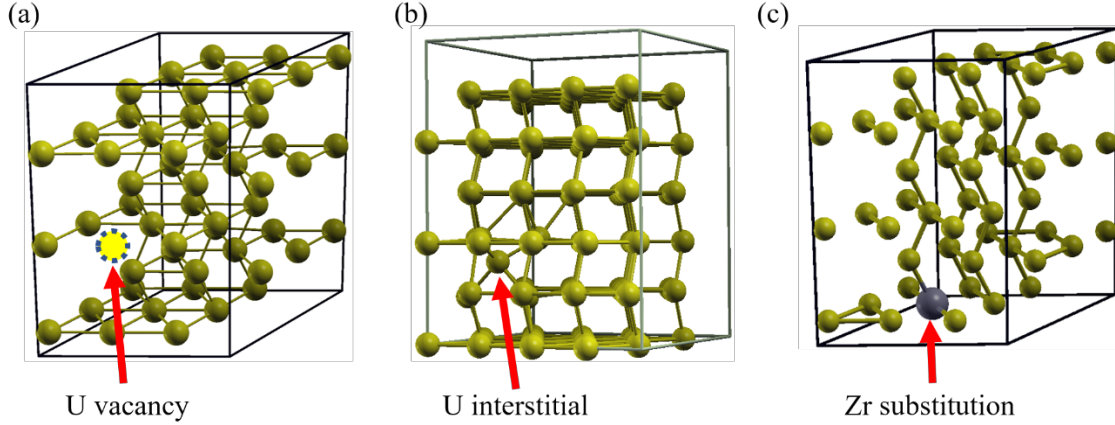


Figure 6. Equilibrium lattice configuration of (a) U-vacancy, (b) U-interstitial, and (c) Zr-substitution defected  $3 \times 3 \times 3$   $\alpha$ -U supercell obtained from DFT calculations. The internal coordinates of the U interstice are (0.49, 0.802, 0.78) based on the basis vector of the conventional cell of  $\alpha$ -U. These values compare well with the other DFT calculation of the U interstice coordinates (0.5, 0.812, and 0.8) [68].

Table 2. Lattice parameters and formation energy of defected  $\alpha$ -U. The vacancy formation energy is calculated using  $E_V = E_{n-1} - \frac{n-1}{n}E_n$  where  $E_{n-1}$  and  $E_n$  is the total energy of the supercell after and before the vacancy is created,  $n = 54$  is the number of atoms in the supercell. Similarly, the interstitial formation energy is calculated using  $E_I = E_{n+1} - \frac{n+1}{n}E_n$  where  $E_{n+1}$  is the total energy of the supercell after the interstitial defect is created. The substitution formation energy is calculated using  $E_S = E_{(n-1)U+Zr} - \frac{n-1}{n}E_n - E_{Zr}$  where  $E_{(n-1)U+Zr}$  is the total energy of the supercell after the interstitial defect is created and  $E_{Zr}$  is the energy of one Zr atom in the  $\alpha$ -U phase.

	a (Å)	b (Å)	c (Å)	Volume/atom (Å <sup>3</sup> )	Formation energy (eV)	References
Perfect	2.817	5.867	4.875	19.99		
U vacancy	2.797	5.83	4.886	19.92	1.9	1.95 [49], 1.86 [68]
U interstitial	2.829	5.847	4.932	20.39	4.9	3.53 [68], 4.42 [69]
Zr substitution	2.871	5.887	4.999	21.13	3.9	

The phonon and electronic thermal conductivities along the [100] direction of three types of defected  $\alpha$ -U are plotted in Figure 7(a)(c)(e). All defects lead to reductions of both  $\kappa_{ph}$  and  $\kappa_e$  since the phonon-defect and electron-defect scatterings hinder thermal transport. For  $\kappa_{ph}$ , the reduction due to the phonon-defect scatterings is gradually diminished as temperature increases. This is because the phonon-defect scatterings are predominant only at low temperatures. As

temperature increases, the phonon-phonon and phonon-electron scatterings become more and more dominant so that the contribution from the phonon-defect scattering to  $\kappa_{ph}$  decreases. However, a reverse trend is observed for  $\kappa_e$  where the reduction due to electron-defect scatterings increases as temperature increases. The temperature dependence of  $\kappa_e$  can be explained by Eq. (7), where the electronic thermal conductivity can be written as  $\kappa_e = L\rho T$ . For electron-defect scatterings, the electrical resistivity  $\rho$  is temperature independent since the electron-defect RT given by Eq. (26) is temperature independent. Therefore,  $\kappa_e$  exhibits almost linear dependence on temperature. The contribution of electron-defect scatterings to thermal conductivity is more prominent at high temperatures. By summing up  $\kappa_e$  and  $\kappa_{ph}$ , the total thermal conductivities along the [100] direction of defected  $\alpha$ -U are obtained and plotted in Figure 7(b)(d)(f). The temperature at which the total thermal conductivity reaches minimum decreases with increasing defect concentration, denoted by the green arrows. This is because at low temperatures, the phonon-defect scattering greatly reduces phonon thermal conductivity which contributes most to the total thermal conductivity. Meanwhile, the electronic thermal conductivity is almost unaffected by the electron-defect scattering. Therefore, the contribution from electrons starts to dominate the total thermal conductivity at a lower temperature when more defects are introduced into the crystal. As a result, the temperature dependence of the total thermal conductivity reverses at a lower temperature.

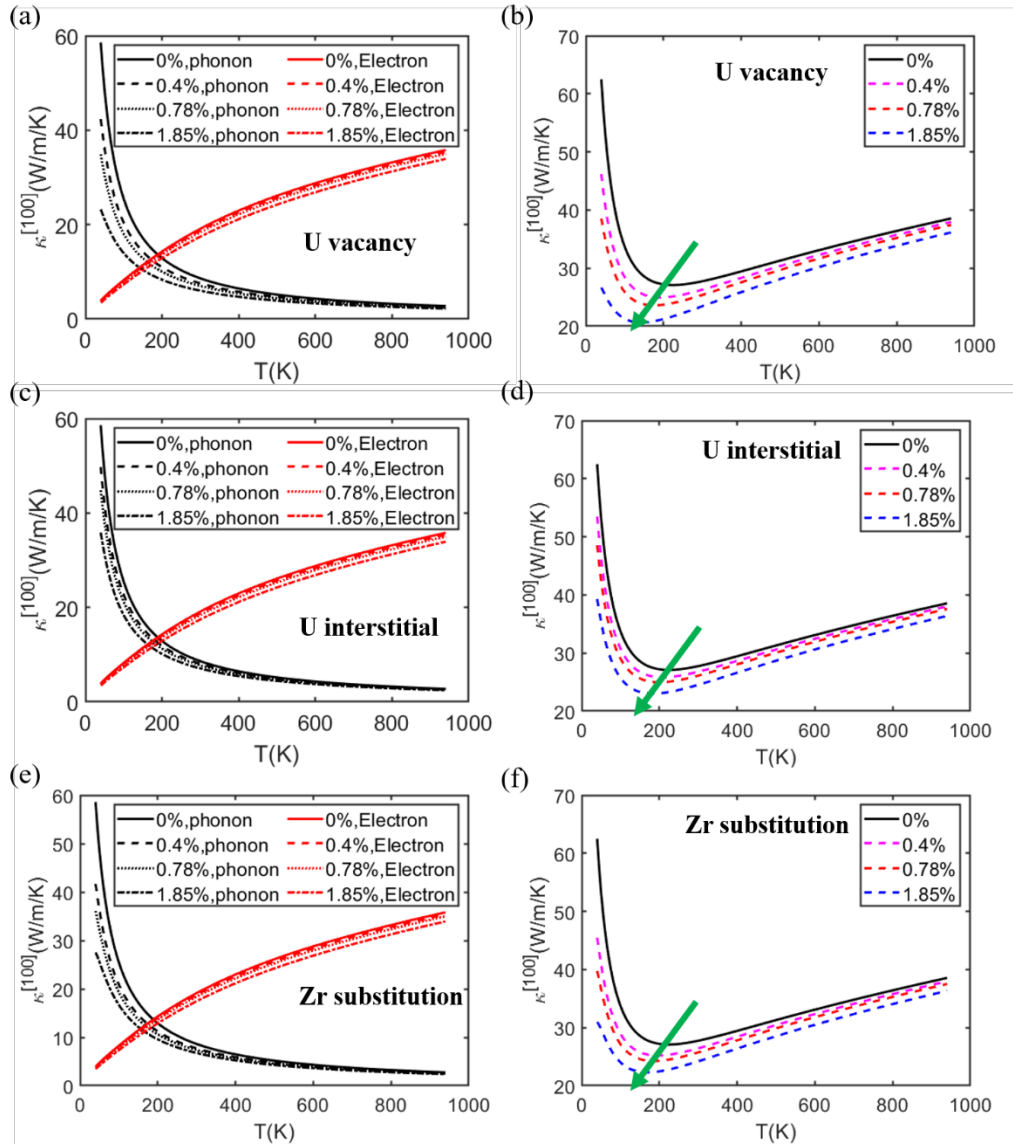


Figure 7. Phonon and electronic thermal conductivity ([100] direction) of (a) U-vacancy, (c) U-interstitial, and (e) Zr-substitution defected  $\alpha$ -U with different defect concentrations. Total thermal conductivity of (b) U-vacancy, (d) U-interstitial, and (f) Zr-substitution defected  $\alpha$ -U.

To quantitatively compare thermal conductivity reduction due to different types of defects at different temperatures, we choose three representative temperatures to show thermal conductivity as a function of defect concentration in Figure 8(a)(c)(e). The effect of defects on thermal conductivity is more prominent at low temperatures. As is shown in Figure 8(a), the U-vacancy defect greatly reduces thermal conductivity at 50 K where 1.85% U-vacancy degrades thermal conductivity from 53.3 W/m/K to 25.3 W/m/K. At room temperature, thermal conductivity

decreases from 27.7 W/m/K to 26.3 W/m/K, 25.4 W/m/K, and 23.5 W/m/K for vacancy concentration of 0.4%, 0.78%, and 1.85%, respectively. At 600 K, the percentage thermal conductivity reductions due to vacancy are almost identical to the reductions at room temperature. Similar observations are made for U-interstitial and Zr-substitutional defects that the largest thermal conductivity reduction occurs at 50 K. This is clearly shown in Figure 8(b)(d)(f), where we plot  $\kappa_{defect}/\kappa_{pure}$  of different defects as a function of temperature. The percentage reduction of thermal conductivity due to defects decreases as temperature is raised. Moreover, the percentage reductions of thermal conductivity due to defects along all three directions are isotropic at high temperatures ( $T > 600$  K) whereas at low temperatures ( $T < 200$  K), the reductions are anisotropic. This is because the thermal conductivity reduction is dominated by phonon-defect scatterings at low temperatures. Since the phonon-defect RTs calculated using Eq. (9) is phonon mode-dependent, the phonon thermal conductivity of defected  $\alpha$ -U is anisotropic. However, at high temperatures, the thermal conductivity reduction is dominated by electron-defect scatterings for which we adopt an isotropic electron-defect RTs in Eq. (26). Therefore, the electronic thermal conductivity reduction by including electron-defect RTs is isotropic.

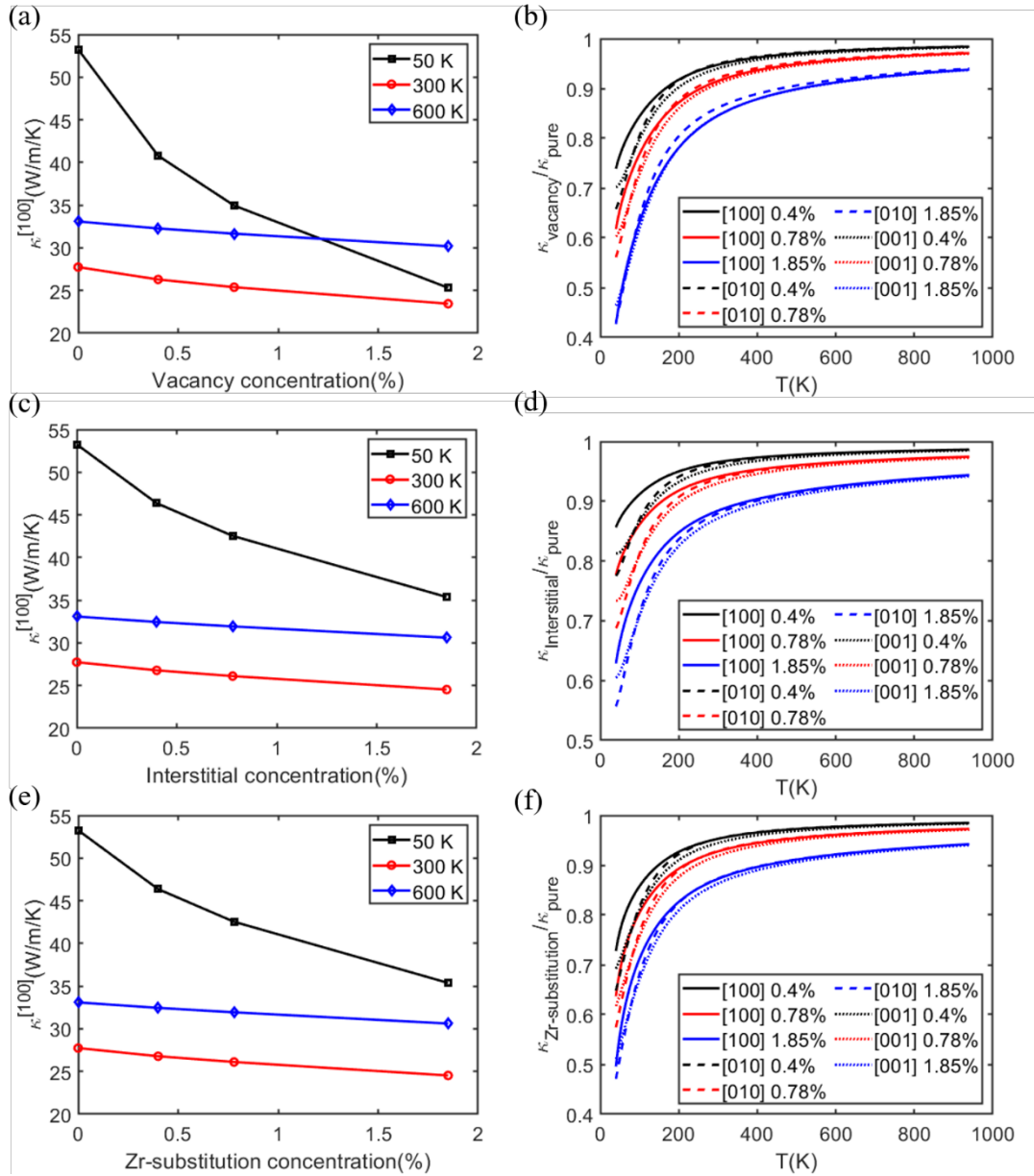


Figure 8. Thermal conductivity (50K, 300K, and 600K) of defected  $\alpha$ -U as a function of (a) U-vacancy, (c) U-interstitial, and (e) Zr-substitution defect concentration. The ratio between the thermal conductivity along all three cartesian directions of defected and pure  $\alpha$ -U as a function of temperature and defect concentration for (b) U-vacancy, (d) U-interstitial, and (f) Zr-substitution.

To understand the effect of defect type on thermal conductivity of  $\alpha$ -U, we show the percentage reduction of room temperature thermal conductivity due to different defects in Figure 9(a). The presence of U vacancy in  $\alpha$ -U has the most substantial influence on thermal conductivity

compared to U-interstitial and Zr-substitution. As is shown in Table 3, the phonon scattering parameter of U-vacancy defect is the largest among three defects, leading to the greatest reduction in phonon RTs. Despite the same mass difference due to U-vacancy and U-interstitial defects, the difference in the stoichiometric average of the lattice and interstitial sites used in Eq. (11) leads to different scattering parameters for these two defects.

Table 3. Scattering parameters  $G$  for each defected type in  $\alpha$ -U with defect concentration  $n_d = 1.84\%$ . The average mass, force constant, and radius per atom site for perfect  $\alpha$ -U are  $M = 238.03 \text{ amu}$ ,  $K = 14.11 \text{ eV/\AA}^2$ , and  $R = 1.69 \text{ \AA}$ , respectively. The interstitial atom has a stoichiometry corresponding to the ratio of interstitial sites to lattice sites [33], which in the  $\alpha$ -U case is 3.5 since there are 7 interstitial sites and 2 lattice sites per unit cell.

Defect type	$\Delta M$ (amu)	$\Delta K$ (eV/ $\text{\AA}^2$ )	$\Delta R$ ( $\text{\AA}$ )	$G$
U-vacancy	-714.087			0.594
U-interstitial	714.087			0.169
Zr-substitution	-146.805	-2.404	0.025	0.389

To gain a better understanding of the effect of point defects on phonon RTs, we show the phonon RTs of pure  $\alpha$ -U and defected  $\alpha$ -U with a concentration of 1.84% at room temperature in Figure 9(b)(c)(d). All three defects lead to a reduction in phonon RTs, most noticeably in the high-frequency phonons – the optical modes. However, since the contributions from the optical modes towards phonon thermal conductivity are small due to their low group velocities, the resulting reduction in thermal conductivity is relatively small. To explore the effect of point defects on thermal transport at different temperature, in Figure 9(d)(e)(f), the phonon RTs of pure and Zr-substitution defected  $\alpha$ -U with 1.84% defect concentration at three representative temperatures – 50 K, 300 K, and 600 K – are shown. The phonon RTs of both pure and defected  $\alpha$ -U decrease with increasing temperatures, leading to the decreasing phonon thermal conductivity with increasing temperature we have already shown in Figure 7(a)(c)(e). Moreover, the reduction in the phonon RTs due to Zr-substitution defects also decreases with increasing temperature, as we compare the difference between the RTs of pure and defected  $\alpha$ -U in at the three temperatures.

This explains why phonon thermal conductivity appears to be not affected by the Zr-substitution defect at around 900 K while reduced by 31.0 W/m/K at 43 K, as is shown in Figure 7(e).

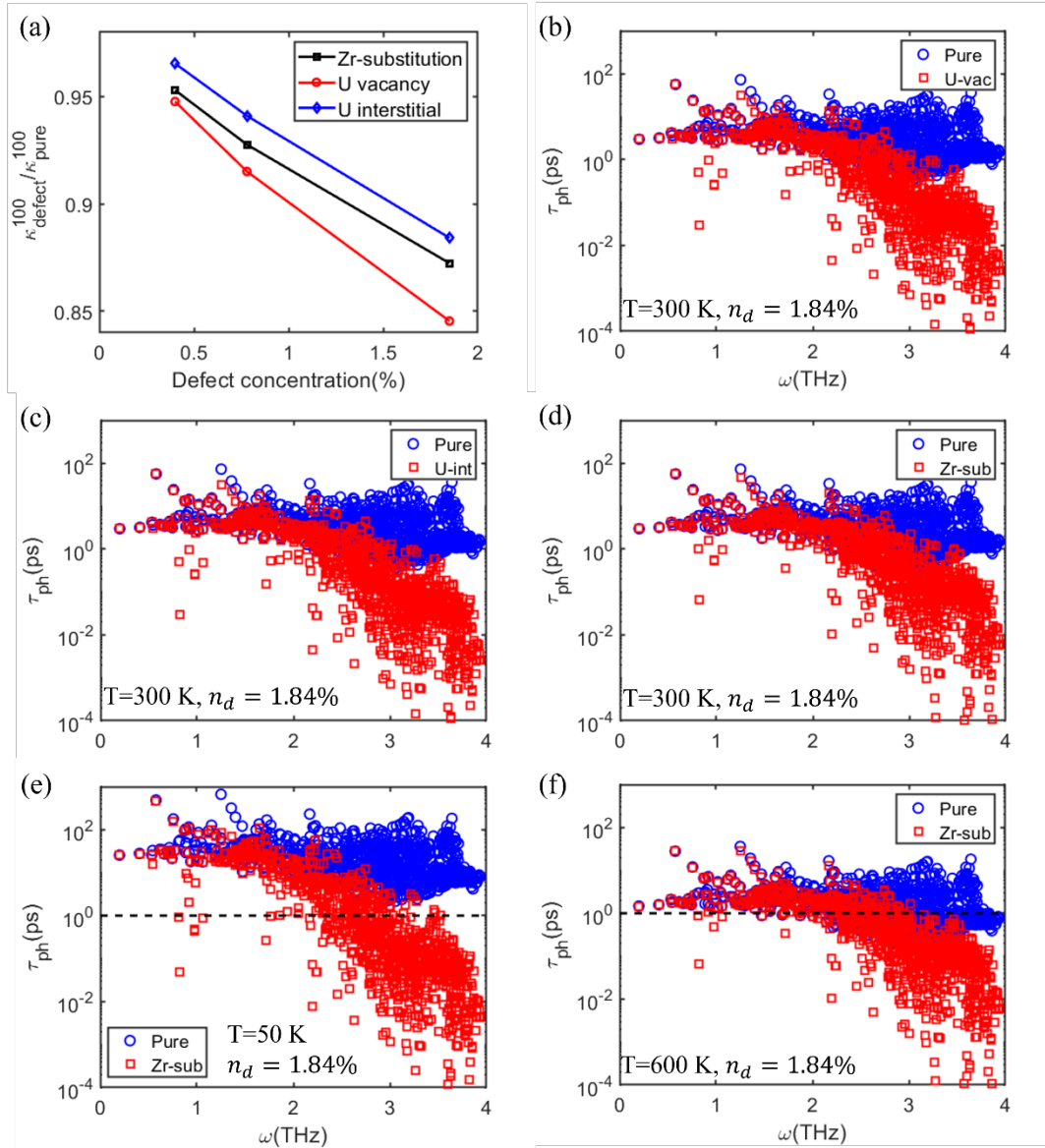


Figure 9. (a) Thermal conductivity ([100] direction,  $T=300$  K) of  $\alpha$ -U as a function of defect concentration for the three types of point defects. Phonon-phonon RTs of pure  $\alpha$ -U and (b) U-vacancy, (c) U-interstitial, and (d) Zr-substitution defected  $\alpha$ -U with a defect concentration of 1.84%. Phonon-phonon RTs Zr-substitution defected  $\alpha$ -U with a defect concentration of 1.84% at (d) 300 K, (e) 50 K, and (f) 600 K. In (d)(e)(f), a general trend of decreasing RTs with increasing temperature can be observed by taking the dashed line as a reference. Also, the difference between RTs of pure and Zr-substitution defected  $\alpha$ -U also becomes smaller as temperature is raised, as more overlapping between the red and blue scatter points appear at high temperature.

## 5 CONCLUDING REMARKS

We have developed a theoretical model of  $\alpha$ -U thermal conductivity which is based on DFT calculation and phonon/electron BTE. The thermal conductivity incorporates both electron and phonon contributions, where the phonon thermal conductivity accounts for the phonon-phonon, phonon-electron, and phonon-defect scattering processes and the electronic thermal conductivity accounts for the electron-phonon, electron-electron, and electron-defect scattering processes. All the parameters are produced using DFT methods, without fitting to any experimental data. The model also goes beyond the traditional Wiedemann-Franz law that assumes constant Lorentz number and adopts temperature-dependent Lorentz number for evaluating the electronic thermal conductivity.

The thermal conductivity values from 43 K to 933 K of pure  $\alpha$ -U produced by our model agrees better with experimental data than the model using the Wiedemann-Franz law. We show that at room temperature and above, electrons are the major heat carriers. Over the entire temperature range, the phonon-phonon scatterings dominate phonon thermal conductivity while the electron-phonon scatterings dominate electronic thermal conductivity. The effects of three different defects – U-vacancy, U-interstitial, and Zr-substitution – on thermal conductivity of  $\alpha$ -U are studied. Defects reduce thermal conductivity significantly at low temperatures where phonon-defect scattering becomes dominant mechanism in thermal transport. The degradation of thermal conductivity along all three crystallographic directions due to defects are almost isotropic. Among the three defects, U-vacancy has the most substantial impact on thermal conductivity due to largest changes in mass and force constants that leads to the greatest reduction in phonon RTs.

Based on the current work, there are several directions for future work. Both the electron-defect and phonon-defect RTs can be calculated using the first-principle methods so as to testify

the classical models used in this work, such as the Klemen's model for phonon-defect RTs. With the RTs data of various scattering processes that we have produced in this work, a transport solution to the coupled electron-phonon BTE would also be promising. For instance, a Monte Carlo scheme can be developed for solving the BTE in metallic materials with the capability of studying electron and phonon transport in complex geometries. Moreover, exploring the effect of defects other than point defects, such as vacancy clusters and dislocation loops, on thermal transport in  $\alpha$ -U is also an intriguing problem.

## **ACKNOWLEDGMENT**

This work was supported by the Center for Thermal Energy Transport under Irradiation and the Energy Frontier Research Center funded by the U.S. Department of Energy, Office of Science, Office of Basic Energy Sciences.

## **DATA AVAILABILITY**

The data that support the findings of this study are available from the corresponding author upon reasonable request.

## **REFERENCES**

- [1] G. H. Lander, E. S. Fisher and S. D. Bader, "The solid-state properties of uranium A historical perspective and review," *Advances in physics*, vol. 43, no. 1, pp. 1-111, 1994.

- [2] K. T. Moore and G. v. d. Laan, "Nature of the 5f states in actinide metals," *Reviews of Modern Physics*, vol. 81, no. 1, p. 235, 2009.
- [3] J. C. Marmeggi, R. Currat, A. Bouvet and G. H. Lander, "Phonon softening in alpha-uranium associated with the CDW transition," *Physica B: Condensed Matter*, vol. 263, pp. 624-626, 1999.
- [4] L. Fast, O. Eriksson, B. Johansson, J. M. Wills, G. Straub, H. Roeder and L. Nordström, "Theoretical aspects of the charge density wave in uranium," *Physical review letters*, vol. 81, no. 14, p. 2978, 1998.
- [5] C. S. Barrett, M. H. Mueller and R. L. Hitterman, "Crystal structure variations in alpha uranium at low temperatures," *Physical Review*, vol. 129, no. 2, p. 625, 1963.
- [6] P. Söderlind, "First-principles elastic and structural properties of uranium metal," *Physical Review B*, vol. 66, no. 8, p. 085113, 2002.
- [7] S. Tan, X. Lai, Y. Zhang and L. Huang, "First-principles study of elastic, band structure and optical properties of uranium," *Journal of Atomic and Molecular Physics*, vol. 25, no. 5, pp. 1028-1034, 2008.
- [8] Y. S. Touloukian, R. W. Powell, C. Y. Ho and P. G. Klemens, Thermophysical properties of matter-the TPRC data series. Volume 1. Thermal conductivity-metallic elements and alloys.(Reannouncement). Data book., Lafayette, IN: Purdue Univ., 1970.

- [9] R. O. A. a. J. A. L. Hall, "The thermal conductivity of  $\alpha$  uranium between 5 and 100 K," *Journal of Low Temperature Physics*, vol. 4, no. 4, pp. 415-419, 1971.
- [10] Y. Takahashi, M. Yamawaki and K. Yamamoto, "Thermophysical properties of uranium-zirconium alloys," *Journal of Nuclear Materials*, vol. 154, no. 1, pp. 141-144, 1988.
- [11] S. Kaity, J. Banerjee, M. R. Nair, K. Ravi, S. Dash, T. R. G. Kutty, A. Kumar and R. P. Singh, "Microstructural and thermophysical properties of U-6 wt.% Zr alloy for fast reactor application," *Journal of nuclear materials*, vol. 427, no. 1-3, pp. 1-11, 2012.
- [12] S. Zhou, R. Jacobs, W. Xie, E. Tea, C. Hin and D. Morgan, "Combined ab initio and empirical model of the thermal conductivity of uranium, uranium-zirconium, and uranium-molybdenum.," *Physical Review Materials*, vol. 2, no. 8, p. 083401, 2018.
- [13] J. M. Ziman, *Electrons and phonons: the theory of transport phenomena in solids*, Oxford university press, 2001.
- [14] N. W. Ashcroft and N. D. Mermin, *Solid state physics*, vol. 2005, new york: London: holt, rinehart and winston, 1976.
- [15] X. Y. Liu, C. R. Stanek and A. D. R. Andersson, "Effect of point defects on the thermal conductivity of UO<sub>2</sub>: molecular," Los Alamos National Lab.(LANL), Los Alamos, NM (United States), 2015.

- [16] A. Resnick, K. Mitchell, J. Park, E. B. Farfán and T. Yee, "Thermal transport study in actinide oxides with point defects," *Nuclear Engineering and Technology*, vol. 51, no. 5, pp. 1398-1405, 2019.
- [17] U. D. Wdowik, V. Buturlim, L. Havela and D. Legut, "Effect of carbon vacancies and oxygen impurities on the dynamical and thermal properties of uranium monocarbide," *Journal of Nuclear Materials*, vol. 545, p. 152547, 2021.
- [18] Y. Li, A. Chernatynskiy, J. R. Kennedy, S. B. Sinnott and S. R. Phillpot, "Lattice expansion by intrinsic defects in uranium by molecular dynamics simulation," *Journal of Nuclear Materials*, vol. 475, pp. 6-18, 2016.
- [19] B. A. Loomis and S. B. Gerber, "Length and electrical resistivity changes of neutron irradiated uranium," *Philosophical Magazine*, vol. 18, no. 153, pp. 539-553, 1968.
- [20] E. Y. Chen, C. Deo and R. Dingreville, "Atomistic simulations of temperature and direction dependent threshold displacement energies in  $\alpha$ - and  $\gamma$ -uranium," *Computational Materials Science*, vol. 157, pp. 75-86, 2019.
- [21] T. M. Tritt, *Thermal conductivity: theory, properties, and applications*, Springer Science & Business Media, 2005.
- [22] W. Li, J. Carrete, N. A. Katcho and N. Mingo, "ShengBTE: A solver of the Boltzmann transport equation for phonons," *Computer Physics Communications*, vol. 185, no. 6, pp. 1747-1758, 2014.

- [23] J. D. Gale, "GULP: A computer program for the symmetry-adapted simulation of solids," *Journal of the Chemical Society, Faraday Transactions*, vol. 93, no. 4, pp. 629-637, 1997.
- [24] A. Matthiessen, "Report of the British Association for the Advancement of Science," 1862.
- [25] T. Feng and X. Ruan, "Higher-order phonon scattering: advancing the quantum theory of phonon linewidth, thermal conductivity and thermal radiative properties," *Nanoscale Energy Transport*, pp. 2-1, 2020.
- [26] A. Ward, D. A. Broido, D. A. Stewart and G. Deinzer, "Ab initio theory of the lattice thermal conductivity in diamond," *Physical Review B*, vol. 80, no. 12, p. 125203, 2009.
- [27] A. Pippard, "CXXII. Ultrasonic attenuation in metals," *The London, Edinburgh, and Dublin Philosophical Magazine and Journal of Science*, vol. 46, no. 381, pp. 1104-1114, 1955.
- [28] P. Lindenfeld and W. B. Pennebaker, "Lattice conductivity of copper alloys," *Physical Review*, vol. 127, no. 6, p. 1881, 1962.
- [29] J. Yang, D. T. Morelli, G. P. Meisner, W. Chen, J. S. Dyck and C. Uher, "Influence of electron-phonon interaction on the lattice thermal conductivity of  $\text{Co}_{1-x}\text{Ni}_x\text{Sb}_3$ ," *Physical Review B*, vol. 65, no. 9, p. 094115, 2002.

- [30] L. G. Radosevich and W. S. WILLIAMS, "Thermal conductivity of transition metal carbides," *Journal of the American Ceramic Society*, vol. 53, no. 1, pp. 30-33, 1970.
- [31] P. G. Klemens, "The scattering of low-frequency lattice waves by static imperfections," *Proceedings of the Physical Society. Section A*, vol. 68, no. 12, p. 1113, 1955.
- [32] R. Gurunathan, R. Hanus, M. Dylla, A. Katre and G. J. Snyder, "Analytical models of phonon–point-defect scattering," *Physical Review Applied*, vol. 13, no. 3, p. 034011, 2020.
- [33] R. Gurunathan, R. Hanus, M. Dylla, A. Katre and G. J. Snyder, "Analytical models of phonon–point-defect scattering," *Physical Review Applied*, vol. 13, no. 3, p. 034011, 2020.
- [34] G. K. Madsen, J. Carrete and M. J. Verstraete, "BoltzTraP2, a program for interpolating band structures and calculating semi-classical transport coefficients," *Computer Physics Communications*, vol. 231, pp. 140-145, 2018.
- [35] A. Sommerfeld, "Zur elektronentheorie der metalle," *Naturwissenschaften*, vol. 15, no. 41, pp. 825-832, 1927.
- [36] H. Smith and H. H. Jensen, *Transport phenomena*, Oxford: Clarendon Press, 1989.

- [37] F. Bloch, "Zum elektrischen Widerstandsgesetz bei tiefen Temperaturen," *Zeitschrift für Physik*, vol. 59, no. 3-4, pp. 208-214, 1930.
- [38] E. Grüneisen, "Die Abhängigkeit des elektrischen Widerstandes reiner Metalle von der Temperatur," *Annalen der Physik*, vol. 408, no. 5, pp. 530-540, 1933.
- [39] D. K. Wagner and a. R. Bowers, "The radio-frequency size effect: A tool for the investigation of conduction electron scattering in metals," *Advances in Physics*, vol. 27, no. 5, pp. 651-746, 1978.
- [40] W. E. Lawrence and a. J. W. Wilkins, "Electron-electron scattering in the transport coefficients of simple metals," *Physical Review B*, vol. 7, no. 6, p. 2317, 1973.
- [41] G. Kresse and J. Furthmüller, "Efficient iterative schemes for ab initio total-energy calculations using a plane-wave basis set," *Physical review B*, vol. 54, no. 16, p. 11169, 1996.
- [42] J. P. Perdew, K. Burke and M. Ernzerhof, "Generalized gradient approximation made simple," *Physical review letters*, vol. 77, no. 18, p. 3865, 1996.
- [43] D. C. Langreth and J. P. Perdew, "Theory of nonuniform electronic systems. I. Analysis of the gradient approximation and a generalization that works," *Physical Review B*, vol. 21, no. 12, p. 5469, 1980.

- [44] S. Baroni, S. D. Gironcoli, A. D. Corso and P. Giannozzi, "Phonons and related crystal properties from density-functional perturbation theory," *Reviews of modern Physics*, vol. 73, no. 2, p. 515, 2001.
- [45] A. Togo and I. Tanaka, "First principles phonon calculations in materials science," *Scripta Materialia*, vol. 108, pp. 1-5, 2015.
- [46] V. I. Anisimov, F. Aryasetiawan and A. I. Lichtenstein, "First-principles calculations of the electronic structure and spectra of strongly correlated systems: the LDA+ U method," *Journal of Physics: Condensed Matter*, vol. 9, no. 4, p. 767, 1997.
- [47] W. Xie, W. Xiong, C. A. Marianetti and D. Morgan, "Correlation and relativistic effects in U metal and U-Zr alloy: validation of ab initio approaches," *Physical Review B*, vol. 88, no. 23, p. 235128, 2013.
- [48] B. Beeler, C. Deo, M. Baskes and M. Okuniewski, "First principles calculations of the structure and elastic constants of  $\alpha$ ,  $\beta$  and  $\gamma$  uranium," *Journal of nuclear materials*, vol. 433, no. 1-3, pp. 143-151, 2013.
- [49] C. D. Taylor, "Evaluation of first-principles techniques for obtaining materials parameters of  $\alpha$ -uranium and the (001)  $\alpha$ -uranium surface," *Physical Review B*, vol. 77, no. 9, p. 094119, 2008.
- [50] J. a.-P. Crocombette, F. Jollet, L. T. Nga and T. Petit, "Plane-wave pseudopotential study of point defects in uranium dioxide," *Physical Review B*, vol. 64, no. 10, p. 104107, 2001.

- [51] A. S. Cooper, "Precise lattice constants of germanium, aluminum, gallium arsenide, uranium, sulphur, quartz and sapphire," *Acta Crystallographica*, vol. 15, no. 6, pp. 578-582, 1962.
- [52] T. Le Bihan, S. Heathman, M. Idiri, G. H. Lander, J. M. Wills, A. C. Lawson and A. Lindbaum, "Structural behavior of  $\alpha$ -uranium with pressures to 100 GPa," *Physical Review B*, vol. 67, no. 13, p. 134102, 2003.
- [53] W. P. Crummett, H. G. Smith, R. M. Nicklow and N. Wakabayashi, "Lattice dynamics of  $\alpha$ -uranium," *Physical Review B*, vol. 19, no. 12, p. 6028, 1979.
- [54] M. E. Manley, G. H. Lander, H. Sinn, A. Alatas, W. L. Hults, R. J. McQueeney, J. L. Smith and J. Willit, "Phonon dispersion in uranium measured using inelastic x-ray scattering," *Physical Review B*, vol. 67, no. 5, p. 052302, 2003.
- [55] M. E. Manley, B. Fultz, R. J. McQueeney, C. M. Brown, W. L. Hults, J. L. Smith, D. J. Thoma, R. Osborn and J. L. Robertson, "Large harmonic softening of the phonon density of states of uranium," *Physical review letters*, vol. 86, no. 14, p. 3076, 2001.
- [56] J. Bouchet, "Lattice dynamics of  $\alpha$  uranium," *Physical Review B*, vol. 77, no. 2, p. 024113, 2008.
- [57] J. Yang, T. Gao, B. Liu, G. Sun and B. Chen, "Ab initio investigations of electron correlation effect and phonon dynamics of orthorhombic uranium," *physica status solidi*, vol. 252, no. 3, pp. 521-531, 2015.

- [58] Y. Baer and J. K. Lang, "High-energy spectroscopic study of the occupied and unoccupied 5 f and valence states in Th and U metals," *Physical Review B*, vol. 21, no. 6, p. 2060, 1980.
- [59] A. S. Antropov, K. S. Fidanyan and V. V. Stegailov, "Phonon density of states for solid uranium: accuracy of the embedded atom model classical interatomic potential," *Journal of Physics: Conference Series*, vol. 946, no. 1, p. 012094, 2018.
- [60] H.-S. Kim, Z. M. Gibbs, Y. Tang, H. Wang and G. J. Snyder, "Characterization of Lorenz number with Seebeck coefficient measurement," *APL materials*, vol. 3, no. 4, p. 041506, 2015.
- [61] G. S. Kumar, G. Prasad and R. O. Pohl, "Experimental determinations of the Lorenz number," *Journal of materials science*, vol. 28, no. 16, pp. 4261-4272, 1993.
- [62] C. Kittel, P. McEuen and P. McEuen, *Introduction to solid state physics*, vol. 8, New York: Wiley, 1996.
- [63] V. O. Eriksen and W. Halg, "The thermal conductivity and electrical resistivity of uranium," *J. Nuclear Energy*, vol. 1, 1955.
- [64] D. A. Howl, "The thermal conductivity of springfields adjusted uranium in the temperature range 160–620 °C," *Journal of Nuclear Materials*, vol. 19, no. 1, pp. 9-14, 1966.

- [65] G. J. Pearson, P. O. Davey and G. C. Danielson, "Thermal Conductivity of Nickel and Uranium," *Proceedings of the Iowa Academy of Science*, vol. 64, no. 1, pp. 461-465, 1957.
- [66] H. E. Flotow, H. R. Lohr, B. M. Abraham and D. W. Osborne, "The heat capacity and thermodynamic functions of  $\beta$ -uranium hydride from 5 to 350 K," *Journal of the American Chemical Society*, vol. 81, no. 14, pp. 3529-3533, 1959.
- [67] Y. Wang, Z. Lu and X. Ruan, "First principles calculation of lattice thermal conductivity of metals considering phonon-phonon and phonon-electron scattering," *Journal of applied Physics*, vol. 119, no. 22, p. 225109, 2016.
- [68] B. W. Beeler, "Atomistic simulations of intrinsic and extrinsic point defects in uranium," Georgia Institute of Technology, 2011.
- [69] G.-Y. Huang and B. D. Wirth, "First-principles study of diffusion of interstitial and vacancy in  $\alpha$  U-Zr," *Journal of Physics: Condensed Matter*, vol. 23, no. 20, p. 205402, 2011.